SERI/PR-0-9372-4
(DE82005675)

AMORPHOUS SILICON SOLAR CELLS

Quarterly Report No. 4 for the Period July 1—September 30, 1981

By
D. E. Carlson
R. S. Crandall
J. Dresner
B. Goldstein
J. J. Hanak
A. R. Moore
D. Redfield
H. E. Schade
H. A. Weakliem

November 1981

Work Performed Under Contract No. AC02-77CH00178

RCA Laboratories
Princeton, New Jersey

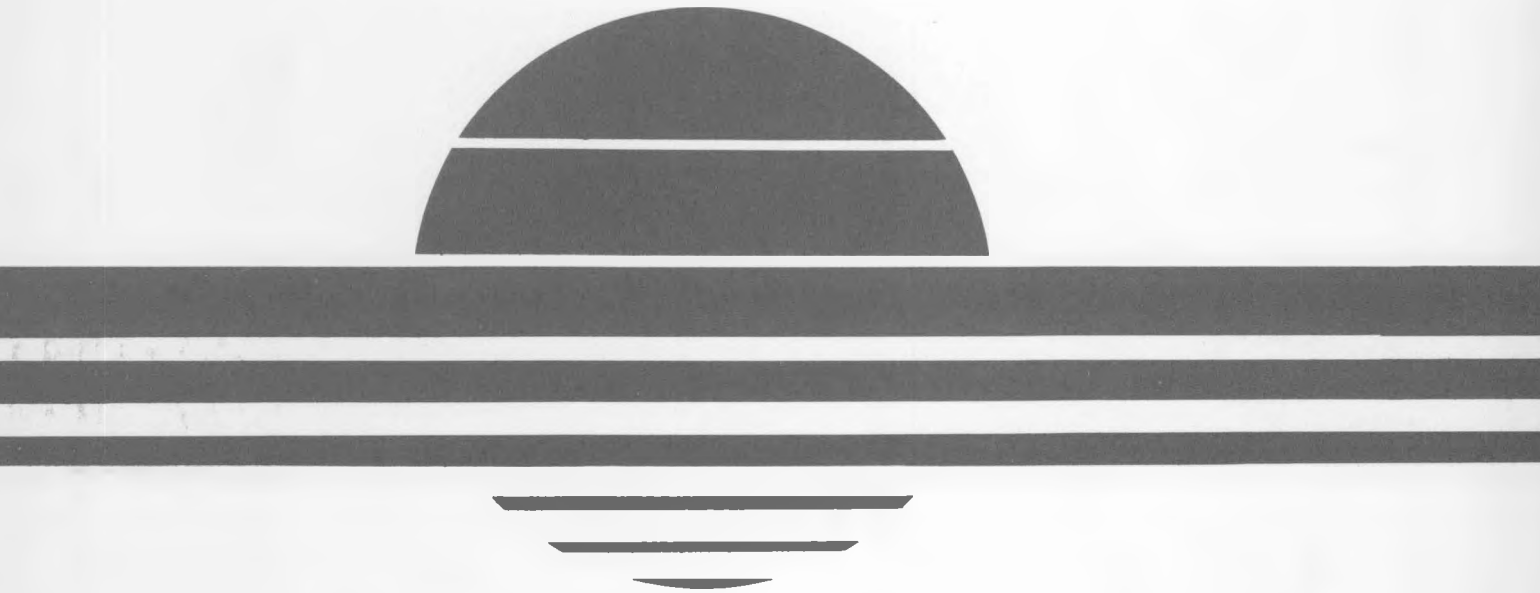

U.S. Department of Energy

Solar Energy

SERI/PR-0-9372-4
(DE82005675)
Distribution Category UC-63b

AMORPHOUS SILICON SOLAR CELLS

Quarterly Report No. 4
for the period 1 July 1981
to 30 September 1981

November 1981

D. E. Carlson
R. S. Crandall
J. Dresner
B. Goldstein
J. J. Hanak
A. R. Moore
D. Redfield
H. E. Schade
H. A. Weakliem

RCA Laboratories
Princeton, New Jersey 08540

Prepared Under Subcontract
No. XG-0-9372-1
for the

Solar Energy Research Institute
A Division of Midwest Research Institute
1536 Cole Boulevard
Golden, Colorado 80401

PREFACE

This Quarterly Report covers the work performed by the Display and Energy Systems Research Laboratory of RCA Laboratories, Princeton, New Jersey, for the period 1 July 1981 to 30 September 1981 under Contract No. XG-0-9372-1. The Staff Vice President is B. F Williams; D. E. Carlson is the Group Head and Project Scientist. The staff members and associate staff personnel who have contributed to the report, and their areas of specialization, are listed below.

D. E. Carlson R. W. Smith	dc Deposition of a-Si:H
*R. S. Crandall J. A. Cioppi	Device Modeling, DLTS
*J. Dresner	Hall Effect Measurements, Diffusion Length Measurements
*A. R. Moore G. R. Latham	Diffusion Length Measurements
*B. Goldstein D. J. Szostak	Surface Photovoltage Profiling, Stability Studies
+J. J. Hanak V. Korsun J. P. Pellicane	rf Deposition of a-Si:H, Structures, Stability Studies
*D. Redfield	Theoretical Modeling
*H. E. Schade Z. E. Smith	Contact Studies
*H. A. Weakliem R. D. Estes	Mass Spectroscopy Studies

*Member of Technical Staff
+Fellow

SUMMARY

Modeling of the free carrier space charge in a-Si:H p-i-n solar cells shows that significant field distortion will occur when the i layer is thicker than $\sim$1 μm.

Compositional analyses have been performed on undoped a-Si:H films that exhibit diffusion lengths greater than 0.5 μm. The SIMS data gave the following impurity concentrations: oxygen ($\lesssim 2.6 \times 10^{19}$ cm^{-3}), nitrogen ($\lesssim 1.4 \times 10^{19}$ cm^{-3}), carbon ($\lesssim 8.5 \times 10^{18}$ cm^{-3}), chlorine ($\lesssim 3.5 \times 10^{16}$ cm^{-3}), boron ($< 10^{17}$ cm^{-3}), and phosphorus ($< 10^{16}$ cm^{-3}). The a-Si:H films typically contain between 6.5 and 9.0 at.% hydrogen.

We have measured hole mobilities as large as 0.2 cm^2/V-s in p type a-Si:H (620-ppm boron) using the Hall effect.

Conversion efficiencies as high as 5.8% have been obtained in p-i-n cells fabricated with a microcrystalline p layer (maximum value of V_{oc} was 920 mV).

Surface photovoltage profiling has been used to show that the n/i interface does not contribute to the open-circuit voltage of cells with the structure ITO/p-i-n/steel. For cells with the structure Al/Ti/n-i-p/cermet/ITO/glass we find that the more stable cells have a relatively large contribution to the built-in potential from the n/i interface and relatively low space-charge densities in the i layer.

TABLE OF CONTENTS

TABLE OF CONTENTS (Continued)

LIST OF FIGURES

SECTION 1.0

INTRODUCTION

A review of the history of hydrogenated amorphous silicon (a-Si:H) and the a-Si:H solar cell can be found in Ref. 1. The present program involves six research tasks: theoretical modeling, deposition and doping studies, experimental methods for the characterization of a-Si:H, formation of solar-cell structures, theoretical and experimental evaluation of solar-cell structures, theoretical and experimental evaluation of solar-cell parameters, and stability studies.

In a separate program, researchers at RCA Laboratories are developing the technology to fabricate large-area a-Si:H solar cells. This program has the objective of developing low-cost, large-area a-Si:H solar panels.

SECTION 2.0

THEORETICAL MODELING

2.1 FIELD NONUNIFORMITY DUE TO PHOTOGENERATED CARRIERS IN A p-i-n SOLAR CELL

There is considerable interest in the effects of space charge on the operation of a-Si:H solar cells [2-6]. The concern has been mainly with the trapped charge arising from the presumed large density of gap states of a-Si:H [7]. In n type Schottky-barrier solar cells, there is ample evidence that trapped charge controls the operation of the cell [5,6]. Nevertheless, in some p-i-n cells there is not significant space charge in the absence of illumination [8]. Furthermore, the space charge under illumination is not associated with trapped charge, but rather with the free carriers themselves [9]. In a solar cell the photogenerated carriers are not replenished at the contacts. This produces, under the action of an applied field, a displacement of holes to one side and electrons to the other side of the cell. This space charge has been shown to give a measurable contribution to the capacitance [9].

In this work, we use a simplified model of a p-i-n solar cell to calculate the transport of photocarriers by solving the coupled continuity and Poisson's equations. From this we draw definite conclusions as to the operating conditions of practical cells. We find that the a-Si:H cell is limited primarily by the hole space charge that predominates because of the low hole mobility.

A simple criterion to determine when space-charge considerations are important is that the field due to the hole space charge is of the order of the applied field. The hole space charge is roughly equal to the product of the short-circuit current and the hole transit time. To get a more accurate criterion and to see how the field and transport are affected by the space charge, one must solve the continuity equations along with Poisson's equation. In general, this set of equations can only be solved numerically. However, there are situations of physical interest where an approximate solution can be obtained. One of these is when diffusion and recombination can be neglected. This is

useful for finding a criterion as to when space-charge considerations are important since diffusion and recombination will tend to reduce the space charge below the value found without them.

It is convenient to define dimensionless densities, fields, and lengths. If G is the generation rate of electron-hole pairs per unit volume per unit time, q the elemental charge, ε the dielectric constant, L the i layer thickness, μ_N the electron mobility, μ_P the hole mobility, E the electric field, P the hole density, N the electron density, x the position coordinate measured from the n-i interface, and $a = \mu_P/\mu_N$, then the normalized field, hole, and electron densities are $e = E/E_c$, $p = P/P_c$, and $n = N/N_c$, respectively, where

$$E_c = L\sqrt{qG/\varepsilon\mu_P}\ ; \qquad P_c = \sqrt{\varepsilon G/q\mu_P}\ ; \quad N_c = \sqrt{\varepsilon G/q\mu_N}. \tag{2-1}$$

In what follows we shall assume that the light is absorbed uniformly throughout the i layer. This permits the continuity equations to be written in the compact form

$$d(ep)/dx = 1; \quad d(en)/dx = -b \tag{2-2}$$

and the Poisson equation becomes

$$\frac{de}{dx} = p - bn \tag{2-3}$$

where $b = \sqrt{a}$. With the boundary condition that photogenerated charges are not replenished at the contacts, $p = o$ at $x = o$ and $n = o$ at $x = 1$, Eqs. 2-2 and 2-3 can be readily integrated. The first integrals of Eq. 2-2 are

$$ep = x; \quad en = b(1-x). \tag{2-4}$$

Substitution of Eq. 2-4 into 2-3 gives a differential equation that can be readily solved for the electric field as a function of position. This field is

$$e^2 = e_s^2 + (1 + a)\,x^2 - 2\,ax. \tag{2-5}$$

The field at x = 0, the surface field (e_s), is found by integrating the electric field across the i layer and setting the result equal to the voltage, V.

The field has a minimum at x = a/(1 + a), which for equal electron and hole mobilities occurs in the center of the i layer. However, for a-Si:H it is more reasonable to take a << 1 which shifts the minimum toward the n-i interface. Conversely, for a >> 1 the minimum of the field is shifted toward the i-p interface.

Since the exact expression for e_s is cumbersome, it will not be reproduced here. However, there are two limiting forms. For a << 1, we find that in the limit of $e_s > 1$, $e_s = V/E_cL$. Therefore, the surface field is V/L and the field in the i layer is nearly uniform and equal to V/L. In the limit $e_s < 1$, $e_s = 2a\ V/E_cL$, and the surface field is 2a V/L which is much less than the average field V/L. In this case the field is nonuniform in the i layer. Thus the meaning of the field E_c is now clear. It separates the high field region with no field distortion from the low field region with significant field distortion. The above implies that the field decreases rapidly once the critical field is reached.

This can be seen in Fig. 2-1 where the normalized field e is plotted across the i layer for different values of e_s for the case of equal electron and hole mobilities (a = 1). It is apparent from the figure that once the average field drops below the critical value E_c, the field in the cell distorts significantly from the average value V/L. The three curves are for a change of only 30% in V/L.

Figure 2-2 shows the more representative situation for a-Si:H. Here a = 0.1.* The small-hole-to-electron-mobility ratio moves the minimum in the electric field close to the n-i interface. However, it also has the effect of making the onset of the field distortion more gradual. This can be seen by the large range of surface fields represented in the figure. Even though the field, e_s, at the n-i interface decreases, the field at the p-i interface increases. This will have an important consequence if recombination of minority carriers at an

*J. Dresner, private communication.

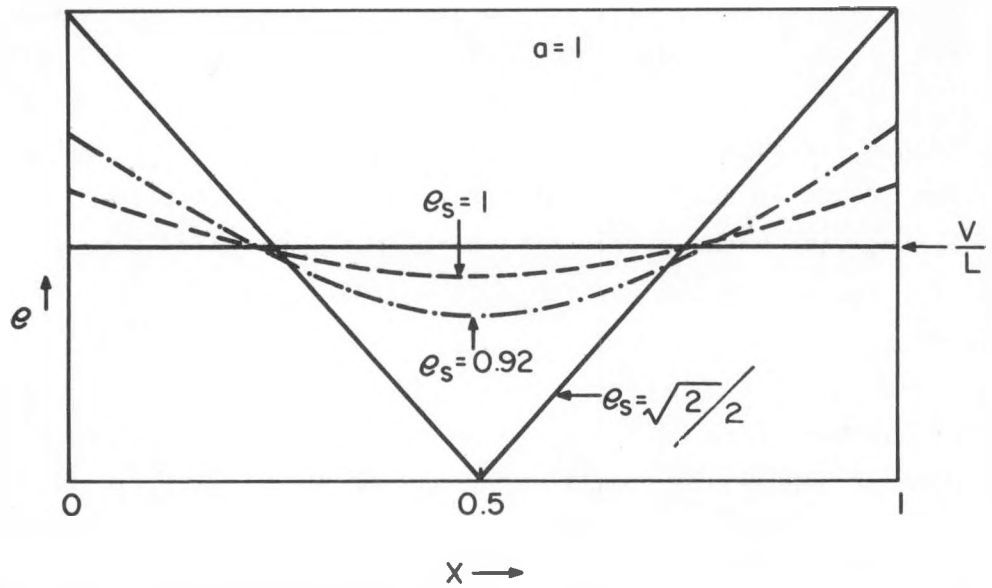

Figure 2-1. NORMALIZED ELECTRIC FIELD AS A FUNCTION OF NORMALIZED DISTANCE ACROSS THE i LAYER FOR a = 1. The average field, V/L, is the solid horizontal line in the center of the graph. The parameter labeling each curve is e_s. The field goes to 0 at the center of the cell when $e_s = 1/\sqrt{2}$

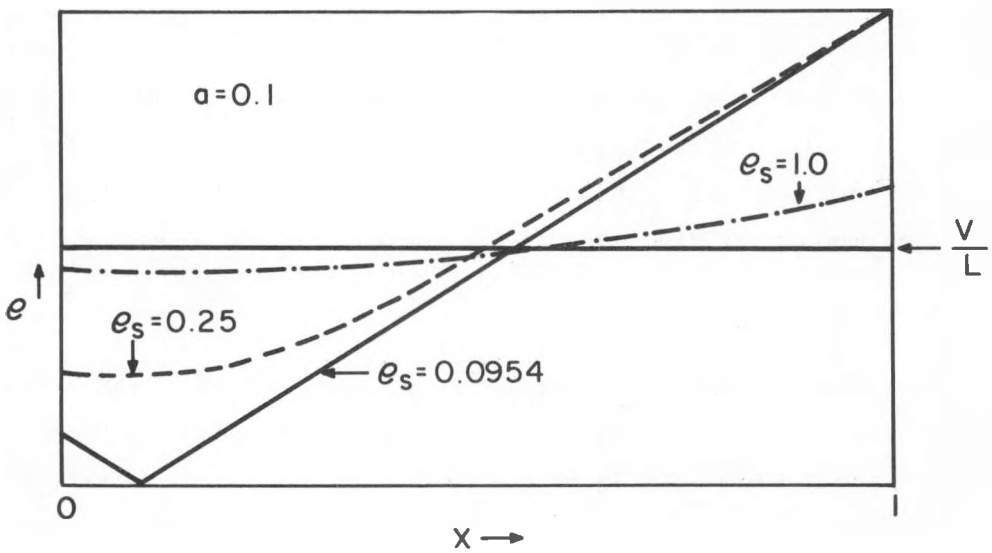

Figure 2-2. SAME PLOT AS Fig. 2-1. Here a = 0.1 and the minimum $e_s = 0.0994$

interface is important. This is because diffusion of the minority carriers toward the interface increases as the field decreases.

Of course, the field distortions cannot be as large as shown in the figure because recombination and diffusion, which have been neglected, will tend to ameliorate the field distortion. This is because the carrier density and its gradient increase as the field decreases. This is shown in Fig. 2-3 where the normalized hole density is plotted as a function of x for $e_s = 2$ and $e_s = 0.1$. When $e_s >> 1$, the field is uniform and p increases linearly with x reaching the maximum value of 1 at x = 1. However, for small e_s, when the field decreases to nearly 0 at x = 0.1, there is a large increase in p and dp/dx.

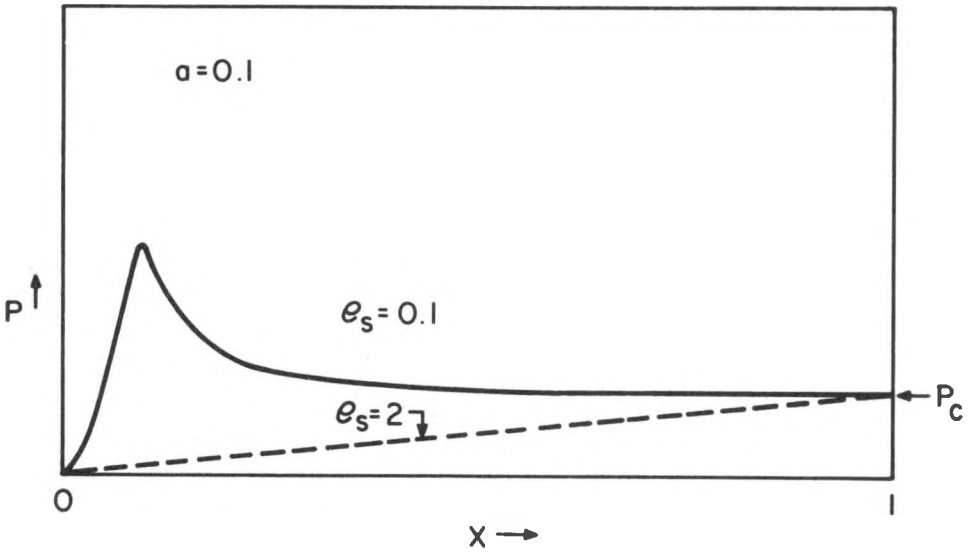

Figure 2-3. NORMALIZED HOLE DENSITY PLOTTED AS A FUNCTION OF NORMALIZED DISTANCE ACROSS THE i LAYER FOR $e_s = 2$ AND $e_s = 0.1$ FOR THE CONDITION a = 0.1. The hole density is P_c at x = 1

It is useful to have a criterion to determine when the field distortion will be significant. One such criterion would be when the minimum field has decreased to zero. Of course the field would not actually drop to zero because at low fields, recombination will become important as well as diffusion and remove the singularity. However, setting the minimum field to zero gives the condition

that $E_c = 2V/L$, which gives meaning to the normalizing field E_c. For a-Si:H the condition becomes

$$L < (4V^2 \varepsilon \mu_p / I_{sc})^{1/3} \qquad (2\text{-}6)$$

where eGL has been replaced by the short-circuit current, I_{sc}. For a typical a-Si:H solar cell $I_{sc} = 0.012$ A, V = 1 V, and $\mu_p = 0.01$ $cm^2/V\text{-}s$.* For these conditions L must be less than about 1 μm to avoid significant field distortion. Actually this is just the region where solar-cell efficiency begins to decrease as a function of thickness [10].

2.2 MODELING OF BAND-TAIL AND GAP STATES

A new effort has been started with the goal of modeling the effects of electron states in energy band-tails and in states deep within the gap on the electrical properties of either undoped or doped a-Si:H. It is widely believed that such states can be sources of space charge which may significantly alter the electric fields in a-Si:H films. This new calculation is based on the best available experimental data on gap states; it provides for two peaks deep in the gap as well as tails on both the valence and conduction bands.

The first phase of this effort is almost complete. It evaluates the temperature dependence of the Fermi energy in the gap for any reasonable values of parameters of the gap states and for various conditions of temperature, doping, etc. This is computationally somewhat difficult because of the complexity of the state density. Preliminary results show that, depending on the doping level, the Fermi energy can increase or decrease as temperature rises.

This knowledge of the Fermi energy is necessary for the next phase in the calculation, which is to determine the distributions of electrons among the states. When the donor-like or acceptor-like character of the different states are assigned, these distributions provide the space-charge information that is sought. In addition, it will be possible to compute the conductivity as a

*J. Dresner, private communication.

function of temperature to test the consistency of the gap-state models with conductivity data.

SECTION 3.0

DEPOSITION AND DOPING STUDIES

3.1 MASS SPECTROSCOPY STUDIES

Mass spectroscopic studies on the ion composition of H_2 and H_2/SiH_4 glow discharges were begun. The initial studies have concentrated on the H_2 rf excited discharge. In addition to H_2^+ and H_3^+, we found considerable quantities of SiH_y^+ and $Si_2H_y^+$ ions. Since no silane was introduced in the chamber, these ions must arise from an etching reaction during which hydrogen atoms or ions react with the solid a-Si:H which was previously deposited on the chamber walls during earlier silane glow discharge runs. The etching occurred with the deposited a-Si:H at room temperature, since no deliberate heating was done. This process is one step of the chemical transport reaction reported for the transport of Si in a H_2 plasma [11]. In that case the reactant Si was a crystalline wafer, and transport occurred by the reaction of the plasma with the cool Si wafer; a deposit of polycrystalline Si occurred on substrates at temperatures as low as 230°C.

During later studies we intend to insert heated substrates and determine the deposited film properties, and we will also compare the silane ion distribution which is produced in a hydrogen discharge with that produced in a silane discharge.

We have begun the design of an assembly which will enable us to measure the composition of a dc discharge at various locations within the discharge. Initially, we will examine the ion composition, and will then study the composition of neutrals using the modulator chamber which was recently constructed.

3.2 IMPURITY ANALYSIS OF AMORPHOUS SILICON WITH A DIFFUSION LENGTH OF 0.55 μm

We have prepared a large number of undoped a-Si:H films with diffusion lengths greater than 0.5 μm by means of several different discharge systems. The

impurity content of these films has been investigated using secondary ion mass spectroscopy (SIMS). A SIMS profile is shown in Fig. 3-1 for an a-Si:H film deposited in a dc(P) discharge; the diffusion length was estimated to be ∿0.55 μm by means of the surface photovoltage technique.

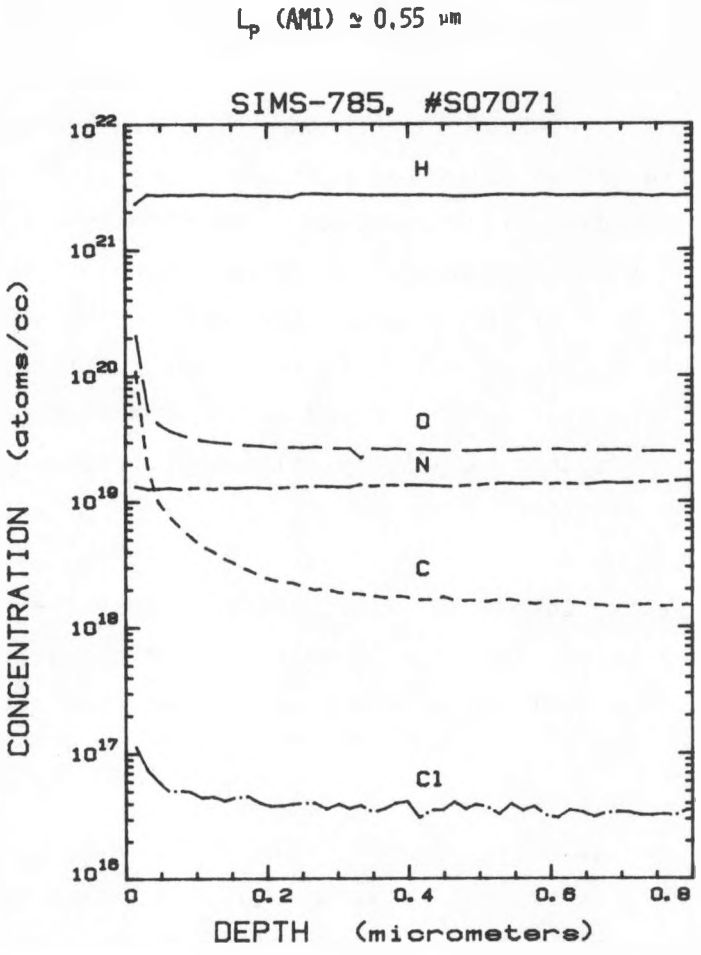

Figure 3-1. A COMPOSITION PROFILE OF AN a-Si:H FILM THAT EXHIBITED A DIFFUSION LENGTH OF ∿0.55 μm (H content is ∿6.7 at.%)

The oxygen concentration (∿2.6X10^{19} cm^{-2}) is typical of a-Si:H films with diffusion lengths greater than 0.5 μm, but the nitrogen concentration (∿1.4X10^{19} cm^{-3}) shown in Fig. 3-1 is somewhat high with other films exhibiting concentrations as low as 6X10^{17} cm^{-3}. The carbon concentrations typically fall in the

range of 1.5 to $8.5X10^{18}$ cm^{-3}. As shown in Fig. 3-1, the chlorine concentration is $\sim 3.5X10^{16}$ cm^{-3}. The boron concentration is less than 10^{17} cm^{-3}, and the phosphorus concentration is less than 10^{16} cm^{-3}.*

Earlier work [12] showed that concentrations of oxygen, nitrogen, and carbon in excess of 1 at.% ($\sim 4X10^{20}$ cm^{-3}) caused a reduction in device performance. Future efforts will concentrate on determining the effects of various impurities on both the diffusion length and the stability.

*From Charles Evans Associates, San Mateo, California.

SECTION 4.0

EXPERIMENTAL METHODS FOR CHARACTERIZING a-Si:H

4.1 LIQUID SCHOTTKY-BARRIER METHOD FOR DIFFUSION LENGTH

During the reporting period, the liquid Schottky-barrier method for implementing the surface photovoltage determination of diffusion length has assumed the role of a general test method of material quality. Fifty or sixty samples have been run, of varying quality, from all of our systems. Values of 0 to 0.6 μm have been observed. We think that values >0.3 μm are needed to make an efficient solar cell. A significant observation has been that there is a definite improvement in diffusion length in the i layer if traces of phosphine from the n^+ layer are removed by long pumping and/or flushing with inert gas during the deposition process.

The computer automation program for the liquid Schottky-barrier diffusion-length equipment is now complete. A complete run at a single-bias light level takes about 2 minutes. Since we normally run at zero bias and 1-Sun bias, the total running time is about 5 minutes. This does not include setup or curve plotting. A complete determination therefore takes approximately 10 minutes. In limited tests, the correlation with the semi-automatic procedure used in the past has been very good.

A set of samples was prepared for illumination through a glass substrate with transparent electrodes of Cr, Mo, and SnO_2:F. The idea was to find out if the hole diffusion lengths in the i layers close to the substrate differed from those measured near the free surface of the film. The experiments failed; in all cases the photovoltages at the illuminated electrodes were much smaller than those generated at the free surface. Another attempt with the same geometry was made with a boron gradient similar to that used in the stable solar cells on steel. This also failed for the same reason. We are now trying to measure the diffusion length on doped layers by illuminating through the free surface.

4.2 HALL EFFECT IN BORON-DOPED a-Si:H

In the last quarterly report we reported results on two samples containing 0.4% of incorporated boron, and μ_H for holes was about 10^{-2} $cm^2V^{-1}s^{-1}$ at room temperature. The significant result was that μ_H changed sign as the temperature was raised through the range 300-500 K; it was p type at room temperature and then changed to n type at about 100°C. This indicates that there are at least two channels for hole conduction.

In this quarter we measured a more lightly doped sample (620 ppm of incorporated boron). The noise level in this more resistive sample was considerably higher. Data reduction was speeded up by using the HP-85 desk computer together with its plotter in the digitizer mode.

As in the previous sample, thermal probe measurements showed p type conductivity from room temperature to 250°C. Near room temperature μ_H is reversed in sign (n type) and is rather large; μ_H = 0.1-0.2 cm^2 V^{-1} s^{-1}. As the temperature is raised, μ_H decreases to about 0.01 at 120°C. Measurements could not be made at higher temperature because of the very high noise level.

All these results are compatible with the idea that hole conduction occurs in more than one set of states. The problem is to find where these states are energetically. We will try to establish an energy scale by combining these results with thermoelectric power measurements. We are now starting to measure a sample with 4% incorporated boron typical of our p^+ layers in solar cells.

We have tried to upgrade the thermal probe apparatus to measure the thermoelectric power Q and get an indication of the location of the Fermi level in these various samples. Many measurements were taken on the Hall samples; while they were qualitatively correct in correlating Q with conductivity they were too inaccurate to yield other information. A new apparatus will have to be built to measure Q accurately.

SECTION 5.0

FORMULATION OF SOLAR-CELL STRUCTURES

5.1 STATUS OF p-i-n CELLS HAVING i LAYERS DEPOSITED FROM AN rf DISCHARGE CONTAINING 5% SiH_4 in H_2

5.1.1 Characteristics of the a-Si:H i Layers

For the study of the deposition of a-Si:H i layers from a SiH_4-H_2 mixture we chose a concentration of 5% SiH_4 in H_2 because at higher concentrations and elevated pressures of 0.5 Torr, considerable dust formation took place. For these conditions and an rf power density of 120 mW/cm^2, a very low optimum T_s range of 140 to 160°C was found. The hydrogen concentration measured by SIMS was $4.5X10^{21}$ as opposed to $3.5X10^{21}$ for material deposited from undiluted silane at about 200°C. The optical gap at T_s of 125°C and 215°C was found to be 1.72 and 1.68 eV, respectively.

5.1.2 Performance of p-i-n Solar Cells

Solar cells consisting of glass/ITO/Pt-SiO_2/p-i-n Si:H/Ti/Al and having a microcrystalline p-Si:H layer yielded a maximum V_{oc} of 920 mV. The highest value of efficiency was 5.5%. Previously we reported a V_{oc} of 933 mV obtained with p layer made with 20% CH_4 in the SiH_4.

5.1.3 Annealing Effects in i Layers Deposited from SiH_4 Diluted in H_2

As mentioned above, cells using i layers deposited from 5% SiH_4 in H_2 favor low deposition temperatures (T_s). We found, however, that annealing of the cells at higher annealing temperatures (T_A) than the T_s causes a decrease in J_{sc}, FF, and η approximately proportional to the difference between T_A and T_s. For samples deposited at doubled gas-flow rates, the decrease was much lower. The reason for this effect might be the release of hydrogen and the accompanying generation of dangling bonds. The result at higher flow rates suggests an involvement of impurities.

5.2 STATUS OF p-i-n CELLS HAVING i LAYERS DEPOSITED FROM rf DISCHARGES IN SiH_4

Most of our a-Si:H solar cells made by rf(C) glow discharge have been deposited from undiluted SiH_4 as described previously. In this method it has been convenient to use a low gas pressure, typically 20 mTorr, primarily to avoid dust formation.

The work, described below, toward the improvement of the i layer has resulted in a substantial increase in performance of 0.1-cm^2 cells made by the rf(C) method: V_{oc} = 820 mV, J_{sc} = 11.6 mA/cm^2, FF = 0.58, and η = 5.8%; the gains occurred mainly in J_{sc}.

5.2.1 Control of Impurities

SIMS depth profiles revealed O and C impurities sometimes exceeding the 10^{21} cm^{-3} level; N and P are at times fairly high. Part of our problem has been the use of low flow rates. When these rates were doubled, the concentration of these impurities decreased by nearly one order of magnitude. Moreover, noticeable improvements in J_{sc} resulted from increasing of the gas-flow rates.

We began monitoring the impurity levels in the deposition chamber by means of a residual-gas analyzer (RGA). Water, (N, CO), and O_2, in that order, are the main impurities adsorbed on the walls.

5.2.2 Increasing the Equilibration Time

The p type layer is deposited at 140°C and the i layer usually higher, necessitating temperature equilibration between the layers. In the past not enough time has been allowed for T_s to equilibrate. This has resulted in a poor quality starting i layer, or one which degrades upon subsequent heating. This change in procedure (increasing the time for equilibration) has been most responsible for the current improvement in the cell performance.

5.2.3 p-i-n Cells With Carbon in the p and n Layers

Since our highest V_{oc} of 933 mV was obtained with a p-i-n cell which had a p layer made with 20% CH_4, we attempted to increase the V_{oc} by incorporating the same amount of carbon in the n layer. The best V_{oc} we obtained with this sample was 883 mV. The cells were more resistive than with an ordinary n type layer apparently due to the more resistive n type film. Hence, carbon in the n layer does not produce beneficial effects.

5.2.4 Concentration of Impurities in Si:H Layers

Because of the low rate of deposition of the microcrystalline-doped layers, impurities such as atmospheric gases and dopant impurities from prior runs tend to concentrate in these layers. For example, a 150-nm-thick p type layer deposited at a rate of 1 nm/min contained about $1.3X10^{20}$ cm^{-3} of phosphorus ($\sim$0.26%) at the start and $2.5X10^{19}$ cm^{-3} (0.05%) at the end of the film. The atmospheric impurities were also abnormally high and decreased with the thickness.

One consequence of the phosphorus contamination was low V_{oc} of $\sim$524 mV for a cell using a microcrystalline p layer made with 0.1% B_2H_6 (and containing about 0.2% B). The boron was probably all compensated by phosphorus. At 0.3% B_2H_6 the V_{oc} increased to 781 mV and at 1.3% to 920 mV.

Another consequence of this effect is probable contamination of the i layer with phosphorus since it is also deposited rather slowly (7 to 11 nm/min). Hence, the contamination would be about 1/5 of the above, approximately low enough not to be detected by SIMS, yet serious enough to limit J_{sc}. It is probably for this reason that cells on glass substrates show a poor blue response when illuminated through the glass side.

5.2.5 Study of Microcrystalline p-Si:H Layers by Raman Scattering

A boron-doped film of Si:H grown in a temperature gradient of ∿130 to 280°C and showing high conductivity (∿1 Ω^{-1} cm^{-1}) in the lower T_s range and low conductivity ($\geq 10^5$ Ω·cm) in the higher T_s range has been studied by Raman scattering at our Zurich Laboratory by E. Steigmeier. He found that the conducting material was a mixture of crystalline and amorphous material, whereas the resistive material was amorphous. Examples of the spectra of the two materials are shown in Figs. 5-1(a) and (b). The formation of microcrystalline material at $T_s \simeq 130$°C is apparently related to the slow deposition rate ($\leq$1.8 nm/min) while amorphous material is created at higher deposition rates (the deposition rate increased with T_s in this study).

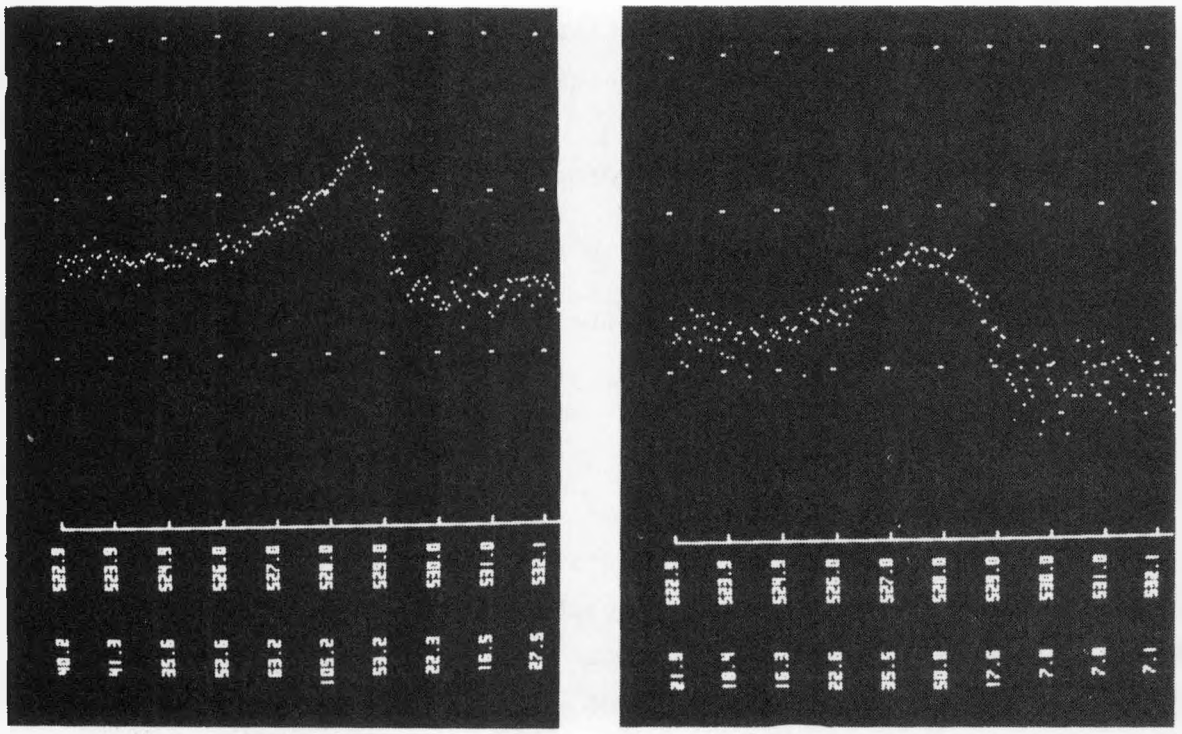

(a) (b)

Figure 5-1. (a) RAMAN SCATTERING SPECTRUM OF A BORON-DOPED Si:H FILM GROWN AT $T_s \simeq 130$°C (microcrystalline)

(b) RAMAN SCATTERING SPECTRUM OF A BORON-DOPED Si:H FILM GROWN AT $T_s \simeq 280$°C (amorphous)

SECTION 6.0

THEORETICAL AND EXPERIMENTAL EVALUATION OF SOLAR-CELL PARAMETERS

6.1 SURFACE PHOTOVOLTAGE PROFILING OF p-i-n SOLAR CELLS

The Photovoltage Profiling Technique has been applied to several different stainless-steel solar cells to study the interface properties. Figure 6-1 shows a typical profile for a good cell (η = 5%) deposited on a stainless-steel substrate. The data shown have been corrected by adding 130 mV to the data in the i layer to account for the sputter-induced upward surface-state band bending, but there is little or no correction in the region of boron tailing. No correction is made in the doped n and p layers since previous work has indicated that there is no photovoltage at room temperature for these layers. From this data we make the following observations:

- The p/i interface produces 530 mV of the total cell voltage of 850 mV.
- The p/i electrical interface (i.e., where $\Delta\phi_s = 0$) penetrates into the i layer a distance of about 1000 Å from the assumed growth interface.
- A 150-mV decrease in the saturated photovoltage ($\Delta\phi_s$) is seen across the n/i interface.
- A 450-mV increase in $\Delta\phi_s$ occurs at the n/ITO interface.

The variation of $\Delta\phi_s$ in the i layer near the p/i interface may be accurately modeled as a one-sided step junction. From Fig. 6-1, the voltage ($\Delta\phi$) and space-charge depth (W) can be obtained by assuming that the depletion width of the p^+/i junction extends into the i layer to the point where $\Delta\phi_s$ becomes constant. Then, $\Delta\phi$ = 530 mV, W = 3200 Å, and N_b can be calculated from Eqs. 6-1 and 6-2.

$$\Delta\phi(x) = \Delta\phi_o\left(1 - \frac{x}{w}\right)^2 \qquad (6\text{-}1)$$

$$\Delta\phi_o = \frac{q\ N_b}{2\ \varepsilon_s} W^2 \qquad (6\text{-}2)$$

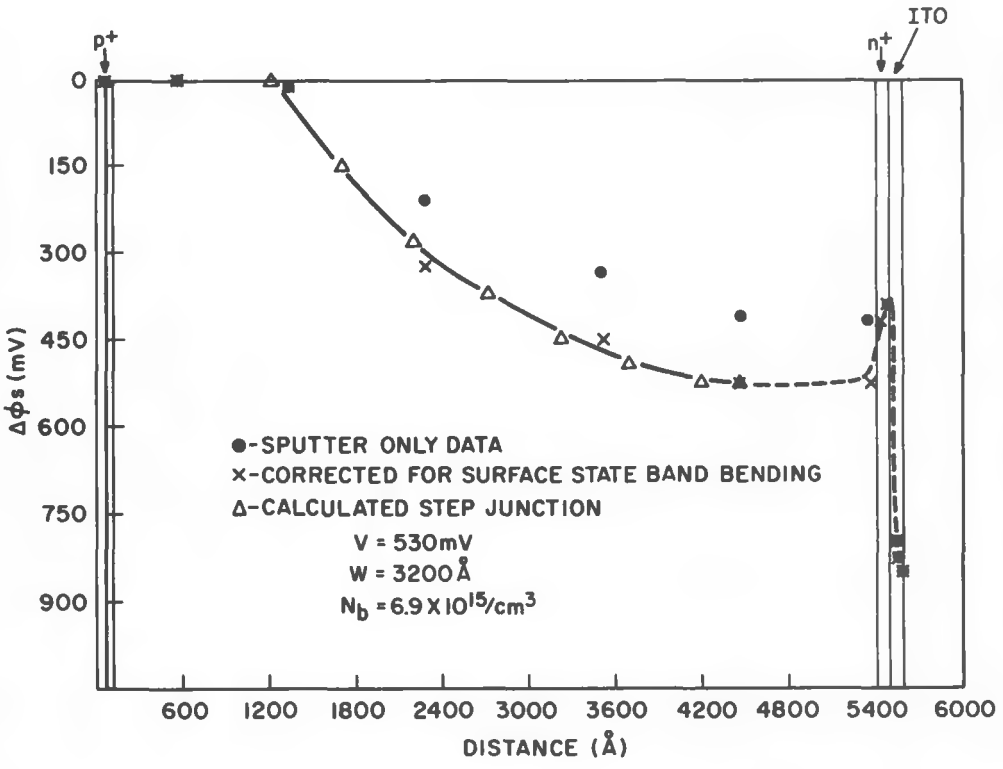

Figure 6-1. A SURFACE PHOTOVOLTAGE PROFILE OF AN a-Si:H SOLAR CELL WITH THE STRUCTURE ITO/n-i-p/steel ($\eta \sim 5\%$)

We find that the electrically active bulk density of states $N_b = 6.9X10^{15}/cm^3$ and the calculated spatial distribution of the potential follow the profiling data quite well as shown in Fig. 6-1. Boron tailing into the i layer (as seen by SIMS) accounts for the displacement of the p/i interface by 1000 Å.

A similar modeling of the n/i and n/ITO interface is not possible for these cells since we have sputtered through these interfaces from the highly doped side, thus removing the dipole and destroying the junction before profiling the space-charge region. To overcome this problem and to look more carefully at the n/i interface, we have profiled a cell deposited on stainless steel with

the reverse structure; that is, ITO/p-i-n/steel. Figure 6-2 shows the results that are listed below:

- Upon removal of the ITO and p layers, the corrected voltage drops to zero. (Indications of a reverse barrier at the p/ITO interface have been observed and will be considered in more detail in future profiling studies of glass substrate cells.)
- If we plot the uncorrected data (i.e., including the surface-state photovoltage), we see a decrease in $\Delta\phi_s$ to zero, begining at 1000 Å from the n/i interface.
- The n/i interface produces no cell voltage.

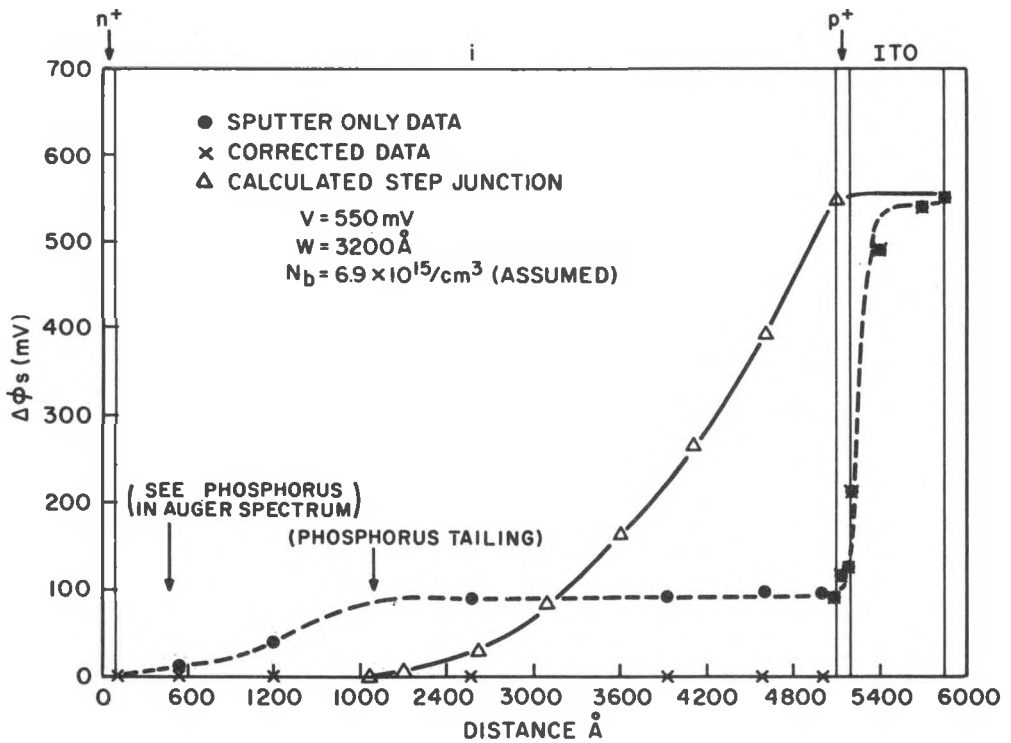

Figure 6-2. A SURFACE PHOTOVOLTAGE PROFILE OF AN a-Si:H SOLAR CELL WITH THE STRUCTURE ITO/p-i-n/steel

Several conclusions can be drawn from these results. First, the n/i interface has no photovoltaic activity. Second, the drecrease in the surface-state

photovoltage near the n/i interface suggests phosphorus tailing into the i layer up to 1800 Å. Finally, the p/i interface produces a voltage of about 550 mV, essentially the same as for a normal ITO/n-i-p/steel cell. To model the p/i interface in Fig. 6-2 as a one-sided step junction, we must assume either N_b or W. Since values for N_b in the i layer have so far ranged from $6\text{-}12X10^{15}/cm^3$, we have chosen N_b for the cell in Fig. 6-2 to be $\sim 7x10^{15}/cm^3$. Then, we calculate W = 3290 Å.

A satisfactory explanation of the profiling data for stainless-steel cells remains clouded by the n/i and ITO/n interfaces. The p/i interfaces all seem straightforward in that (1) they can be modeled as a step-junction with all the space-charge width residing in the i (low doped) side of the junction, (2) the junction height and depletion width directly measurable, and (3) the resulting space charge density ρ is in good agreement with values of N_c (carrier density or effective gap state density) as measured by others. However, several features of the n interfaces are surprising and, if confirmed, can bear very importantly on solar-cell operation.

For one thing, we have indications that there is no or little voltage developed across the n/i interface, and, in fact, there may be a barrier to current flow present when ITO is present. For another, we always see some voltage developed across the ITO/n interface. The thickness of the n layer may be important since that may determine to what extent it becomes depleted when it must supply electrons to support the dipoles formed by the interfaces. Perhaps the single most important unknown factor in modeling the ITO/n/i region is how or where the energy bands join for the ITO/a-Si interface, since this determines the nature of the space charge and the Fermi level changes across these interfaces.

We are in the process of using the results described above to point the way to a definitive series of experiments involving photovoltage profiling, spectral dependence, and intensity dependence applied to <u>single</u> interfaces (and multiple interfaces where appropriate) to try to clarify the problems impeding our understanding of the interfaces in the basic solar-cell structures.

6.2 CONTACT RESISTANCE STUDIES

Based on a previous comparison of flow geometries suitable for constant resistivity measurements, we now have concentrated on a sandwich arrangement ("vertical" flow) [13]. Initially, the following contact combinations were studied: stainless steel/p, ITO/p, and ITO-cermet/p, where p refers to p type a-Si:H.

For these combinations, the p type a-Si:H is deposited onto the contact material under study ("bottom contacts") just as it is done for actual solar-cell structures; a Cr contact ("top contact") is then evaporated onto the p layer to complete the sandwich structure.

In order for us to compare different contact materials, the p type a-Si:H deposition onto these various materials was performed in the same run. Two sets of samples, with a-Si:H p layers grown in a dc and rf glow discharge, have led to the following results:

- The measured sandwich resistance is practically independent of the p layer resistivity (5 to 250 Ω·cm). For a given contact combination, we thus obtain similar sandwich resistances for the two different deposition runs, and also along a sample with varying resistivity, graded from microcrystalline to amorphous.
- There is, however, a proportionality between the sandwich resistance and the sheet resistance of the bottom contact material.
- The sandwich resistance varies inversely with the geometrical contact area, but not directly in inverse proportionality, as one should expect for pure interface resistances.

From the latter two results, we conclude that the measured sandwich resistance contains a contribution from the sheet resistance of the bottom contact material which leads to current crowding and a nonuniform current density across the interfaces. The sheet resistance of the top contact material (Cr) of these samples was found to be negligible. We have developed two methods to calculate the actual interface resistance:

- By approximating the sandwich resistance as a network of parallel (interface) and series (contact material) resistances, one can calculate

from the measured sandwich resistance the true interface resistivity, provided one also knows (by separate measurement) the sheet resistance of the bottom contact material.

- With the sandwich resistances measured for two different contact areas, one can calculate the interface resistivity with a transmission line model (TLM) [14]. With this model, one can also determine the sheet resistance of the bottom contact material as an independent check of the experimental value.

Based on these two methods, we have calculated the contact resistivities listed in Table 6-1. These resistivities are independent of the contact area, i.e., the total contact resistance, calculated with the network model, is inversely proportional to the contact area. Also shown in Table 6-1 are the measured and calculated sheet resistances of the bottom contact material.

Table 6-1. TOTAL CONTACT RESISTIVITY OF SANDWICH STRUCTURES AND SHEET RESISTANCE OF THE BOTTOM CONTACT MATERIAL

Structure	ρ_c total ($\Omega \cdot cm^2$)		R_b ($\Omega/\square$)	
	Network	TLM	TLM	Measured
Stainless Steel/p/Cr	4	5	16	16
ITO/p/Cr	14	17	40	20
Cermet/p/Cr	15	20	254	190

The contact resistivities shown in the Table refer to the sum of the bottom and top contact, and thus represent upper limits for the stainless steel/p, ITO/p, and cermet/p interfaces.

Efforts are under way to deduce the individual contact resistivities of the bottom and top interfaces. While the chosen sample geometry allows us to separately measure a voltage drop across the bottom and top interface, the interpretation of these voltage drops is complicated, since for the present samples the interfaces are not equipotential planes, due to the current crowding

mentioned above. Therefore, samples are now being prepared with additional highly conductive layers below or above the actual bottom and top contact material, respectively, in order to obtain a more uniform current density distribution through the interfaces.

SECTION 7.0

STABILITY STUDIES

7.1 SURFACE AND INTERFACE STUDIES

We have applied the photovoltage profiling technique to solar cells deposited on glass substrates. In this structure the ITO is in contact with the p layer, and the n layer is grown thicker than for the stainless-steel cells since light does not enter through this side of the cell. Figures 7-1 and 7-2 show two profiles, one of a good, stable cell ($\eta \sim 4\%$) and one of a poor, unstable cell ($\eta \sim 2\%$). Both cells were profiled in an annealed condition so that differences due to light soaking are not present. Also, the i layer of the poor cell was about 700 Å thicker. The corrected data takes into account the fact that in the i region there is a -130-mV correction to $\Delta\phi$ due to surface-state band-bending, but in the region of observed boron-tailing (about 600 Å from the p^+ region into the i region for Fig. 7-1; less for Fig. 7-2), this correction is close to zero.

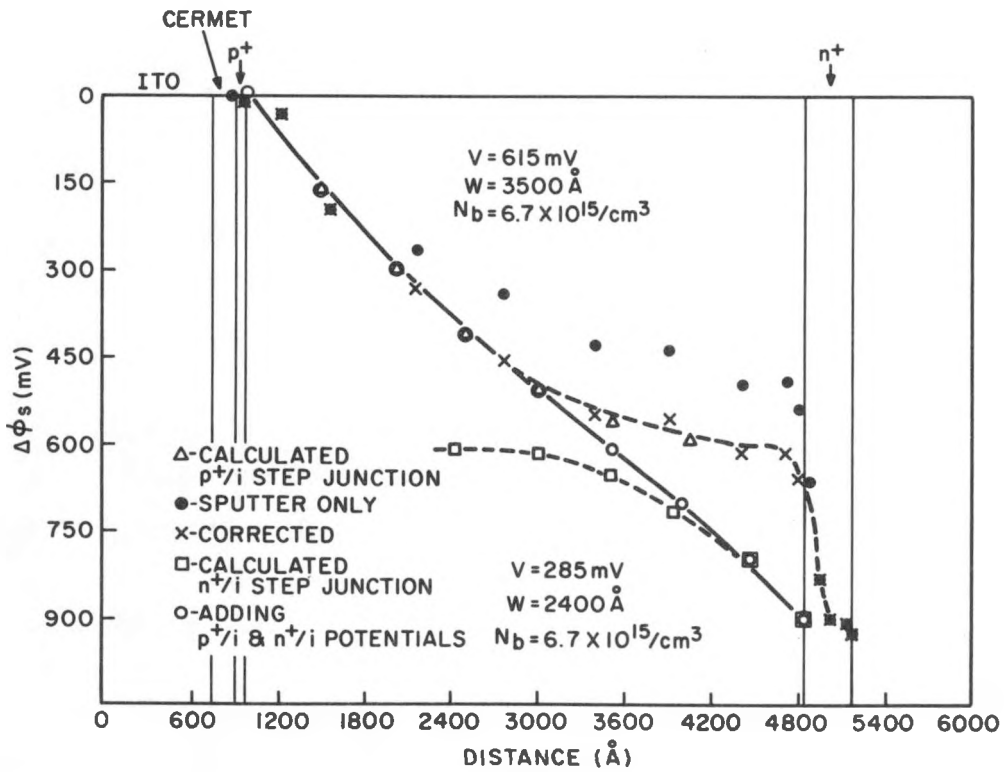

Figure 7-1. A SURFACE PHOTOVOLTAGE PROFILE OF A STABLE a-Si:H SOLAR CELL WITH THE STRUCTURE Al/n-i-p/ITO/glass ($\eta \gtrsim 4\%$)

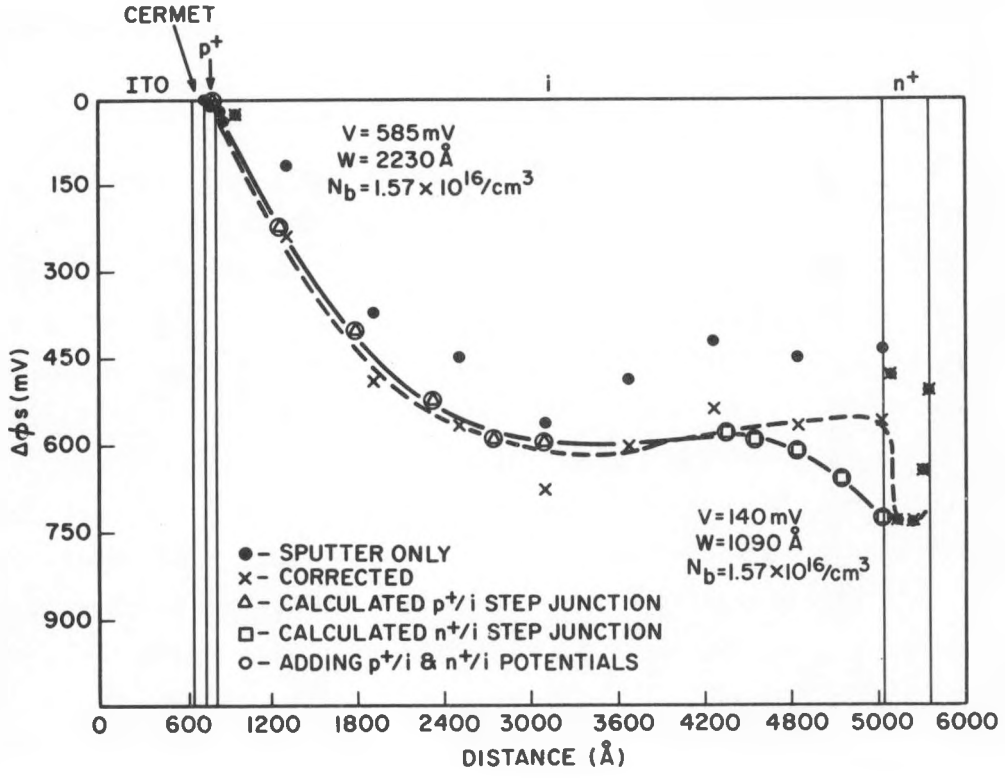

Figure 7-2. A SURFACE PHOTOVOLTAGE PROFILE OF AN UNSTABLE a-Si:H SOLAR CELL WITH THE STRUCTURE Al/n-i-p/ITO/glass ($\eta \sim 2\%$)

To interpret this data we again assume a one-sided step junction for the p/i interface with the voltage and space-charge width experimentally determined at the point where $\Delta\phi_s$ becomes constant, and with N_b and the potential distribution calculated from Eqs. 6-1 and 6-2.

Although both cells have nearly the same voltage for this p/i interface, the poor cell has a smaller W and a higher bulk state density. Unlike the steel cells (see Section 6.1), the n/i interface in these glass cells produces a jog in $\Delta\phi_s$ in the direction expected for a normal n/i interface. Assuming that this is also a step junction and that N_b is uniform in the i layer, we can calculate W and the potential distribution as shown. We see the good cell has both a larger voltage across the n/i interface and a larger W. The final profiles in Figs. 7-1 and 7-2 (solid lines) show the good cell to have a larger

total voltage due to a better n/i interface and the bad cell to have a 1500-Å dead layer due to a higher bulk state density and thus smaller space-charge widths. This dead layer feature will be enhanced in forward bias illumination. Two other indicators of this dead layer can be found in the spectral dependence of the photovoltage. First, the ratio of red to blue response is signficantly larger in the poor cell indicating poor hole transport across the i layer. Second, the threshold and magnitude of below band gap photovoltage responses suggest a larger number of photoactive gap states in the poor cell.

7.2 LIGHT-INDUCED DEGRADATION OF p-i-n CELLS DEPOSITED FROM SiH_4 DILUTED IN H_2

We tested the stability of p-i-n cells deposited from 5% SiH_4-H_2 mixtures. A sample deposited in a T_s range of 145 to 262°C (with V_{oc} = 920 mV and η = 5.26%) was subjected to 67 hours of AM1 illumination. The efficiency of all cells degraded, degradation being highest for the lowest T_s (48%) and lowest for the highest T_s (28%).

Thus, it appears that amorphous silicon deposited from 5% SiH_4-H_2 mixtures at low temperatures is a very unstable material as it is easily degraded by light or by heat (see Section 5.1.3).

The deposition of a-Si:H from more concentrated gas mixtures or undiluted SiH_4 appears to offer a better prospect, as the optimum T_s moves to a higher range where greater stability occurs.

SECTION 8.0

REFERENCES

1. Carlson, D. E. Solar Energy Materials 3, 503 (1980).
2. Dalal, V. Solar Cells 2, 261 (1980); also A. Rothwarf in a paper presented at the 15th IEEE Photovoltaic Specialists Conference, Orlando, Florida, May 1981.
3. Tiedje, T., Wronski, C. R., Abeles, B., and Cebulka, J. M. Solar Cells 2, 301 (1980).
4. Madan, A. Solar Cells 2, 277 (1980).
5. Debney, B. T. Solid State Electron. Devices 2, S-15 (1978).
6. Williams, R. and Crandall, R. S. RCA Review 40, 371 (1979).
7. Madan, A. and Lecomber, P. G. J. Noncrystalline Solids 20, 239 (1976).
8. Crandall, R. S. RCA Review, to be published.
9. Carlson, D. E. et al. Quarterly Report No. 3, SERI/PR-0-8254-3, prepared under Subcontract No. XJ-9-8254, June 1980.
10. Hamakawa, Y., Okamoto, H., and Nitta, Y. 14th IEEE Photovoltaic Specialists Conference, San Diego, California, January 1980.
11. Igbal, Z., Webb, A. P., and Veprek, S. Appl. Phys. Lett. 36, 163 (1980).
12. Carlson, D. E. J. Amer. Vac. Soc., to be published.
13. Carlson, D. E. et al. Quarterly Report No. 3, SERI/PR-0-9372-3, prepared under Subcontract No. XG-0-9372-1, August 1981, pp. 36-39.
14. Berger, H. H. Solid State Electron. 15, 145 (1972).

☆U.S. GOVERNMENT PRINTING OFFICE: 1981-740-145/2785